Acta Cryst. (1979). B35, 1–10

Mixed-Valent $Ba_2Bi^{3+}Bi^{5+}O_6$: Structure and Properties *vs* Temperature

BY D. E. COX*

Physics Department, Brookhaven National Laboratory, Upton, New York 11973, *USA*

AND A. W. SLEIGHT

Central Research and Development Department, E. I. duPont de Nemours and Company, Wilmington, Delaware 19898, *USA*

(*Received* 1 *June* 1978; *accepted* 1 *August* 1978)

Abstract

The structure of the ordered perovskite-like compound $Ba_2Bi^{3+}Bi^{5+}O_6$ has been determined by X-ray and neutron powder diffraction techniques over the temperature range 295–723 K. A first-order transition from monoclinic to rhombohedral occurs at about 405 K. Profile refinement of the neutron data shows that a satisfactory description of both structures can be given in terms of tilting of rigid BiO_6 octahedra, the transition corresponding to an abrupt change in the tilt axis from pseudocubic [110] to [111]. The respective space groups are $I2/m$ and $R\bar{3}$, the Bi^{3+} and Bi^{5+} ions retaining their ordered arrangement in the rhombohedral phase. The analysis also reveals considerable anisotropy in the thermal vibrations of the oxygen ions. The r.m.s. amplitude perpendicular to the Bi—O bond is about double that along the bond, consistent with the rigid-octahedron picture. The data further indicate that there is a transition to cubic symmetry at about 750–800 K. The 405 K transition in $BaBiO_3$ is strikingly similar to the 205 K transition in $PrAlO_3$.

1. Introduction

Cations of Group V*a* are generally in the oxidation state +5 or +3, the latter being frequently referred to as lone-pair cations. A controversy has existed for many years concerning the oxidation state of Sb in halides of the type $A_2^{1+}SbX_6^{1-}$ (Robin & Day, 1967). Originally, these compounds were widely regarded as examples of tetravalent Sb. Initial structural work indicated that such phases were isomorphous with $A_2Pb^{4+}X_6$ and $A_2Pt^{4+}X_6$ compounds and that there was only one crystallographic site for Sb, which must then be Sb^{4+}. However, careful crystallographic studies by Lawton & Jacobson (1966) have shown that the valence situation in $(NH_4)_2SbBr_6$ is $(NH_4)_4Sb^{3+}Sb^{5+}Br_{12}$. Recent Sb Mössbauer studies (Longworth & Day, 1976) have confirmed that $A_2^{1+}SbX_6^{1-}$ compounds contain a mixture of Sb^{3+} and Sb^{5+} rather than Sb^{4+}.

A similar controversy has existed for $BaBiO_3$. Some workers (Scholder, Ganter, Glaser & Merz, 1963; Shuvaeva & Fesenko, 1969; Fesenko, Shuvaeva & Gol'tsov, 1972; Venevtsev, 1971) have assumed that the mixed-valent situation $Ba_2Bi^{3+}Bi^{5+}O_6$ pertains. Others (de Hair & Blasse, 1973) have suggested that this compound represents an example of Bi^{4+}. Still others (Nakamura, Kose & Sata, 1971) considered the controversy unresolved. The discovery of superconductivity in the $BaBiO_3$–$BaPbO_3$ system (Sleight, Gillson & Bierstedt, 1975) has made this controversy of even greater interest. It is not feasible to answer this valency question by Mössbauer spectroscopy, and X-ray diffraction will not readily give the required accuracy of oxygen positions.

A preliminary account of the room-temperature structure of $BaBiO_3$ determined by neutron profile refinement has been given in a recent paper (Cox & Sleight, 1976*a*). From this, it was concluded that the true unit cell was monoclinic and contained four formula units of $BaBiO_3$. A striking feature of this structure is that the Bi atoms occupy two quite distinct sites with average Bi—O distances of 2·28 and 2·12 Å respectively, which is consistent with the valence formulation $Ba_2Bi^{3+}Bi^{5+}O_6$.

Confirmation of this structure has very recently been obtained in an independent neutron diffraction study by Thornton & Jacobson (1978). Further evidence of the mixed-valent character of $BaBiO_3$ has been provided by X-ray photoelectron spectroscopy (Orchard & Thornton, 1977), and comparison of the lattice constants of a number of ordered perovskites (Nakamura & Choy, 1977).

However, two other papers have recently appeared with different conclusions. Khan, Nahm, Rosenberg & Willner (1977) conclude from X-ray powder data that the symmetry is orthorhombic, with two formula units of $BaBiO_3$ per unit cell, while Arpe & Müller-

* Research supported by the Division of Basic Energy Sciences, Department of Energy, under Contract No. EY-76-C-02-0016.

Buschbaum (1977) conclude from a single-crystal X-ray study that the correct cell is tetragonal and contains one formula unit of $BaBiO_3$. In both proposed structures, the Bi atoms are assigned to a single set of sites.

The present paper describes a neutron diffraction study of $BaBiO_3$ as a function of temperature, and also confirms our previous findings. The results also illustrate very well the simple geometrical concepts developed by Megaw (1972, 1973) and Glazer (1972, 1975) for characterizing perovskite structures and phase transitions.

2. Experimental

Polycrystalline $BaBiO_3$ was prepared by heating in air at 1073 K an intimate 1:1 mixture of $Ba(NO_3)_2$ and $Bi(NO_3)_3.5H_2O$ using a gold container. X-ray and neutron diffraction and microscopic examination revealed the golden-brown product to be single phase. The formula was confirmed by chemical analysis, the calculated and observed percentages for Ba, Bi, and O being 35·23 *vs* 35·6, 53·00 *vs* 52·9, and 12·17 *vs* 12·14 respectively.

Crystals of $BaBiO_3$ were grown hydrothermally. A charge of 0·356 g BaO_2, 0·664 g $Ba(OH)_2.8H_2O$, and 0·980 g Bi_2O_3 was sealed in a gold tube ($\frac{1}{2}''$ diameter × 5″ long) (12·7 × 127 mm) by welding. This tube was heated at 973 K for 8 h with 300 MPa external pressure. The product was multiphase but contained many golden cubes up to 1 mm on an edge. The X-ray powder pattern of these cubes was that of $BaBiO_3$.

Electrical-resistivity measurements were performed on $BaBiO_3$ using four Ag contacts. Crystals were used over the temperature range 4·2 to 473 K, and a sintered pellet was used from 298 to 973 K.

Differential scanning calorimetry (DSC), differential thermal analysis (DTA), and thermal gravimetric analysis (TGA) experiments were performed in air using a DuPont 990 thermal analyzer. Magnetic susceptibility was measured by the Faraday method.

X-ray powder patterns at 298 K were obtained both with a Hägg–Guinier camera using Cu $K\alpha$ radiation and an internal standard of KCl (a = 6·2931 Å) and with an IRDAB-XDC-700 Guinier camera using Cr $K\alpha_1$ radiation. X-ray data above room temperature were obtained using a Nonius high-temperature Guinier camera.

Neutron data were collected at several temperatures from the same pellet of material used in the previous room-temperature study (Cox & Sleight, 1976*a*). Pyrolytic graphite in the 002 and 004 reflection positions was used as monochromator and analyzer respectively. The neutron wavelength was 2·354 Å, higher-order components being removed with a pyrolytic-graphite filter. The $\lambda/2:\lambda$ intensity ratio was found to be less than 0·1%. Collimation was set at 20, 40, 40 and 10′ for in-pile, monochromator–sample, sample–analyzer and analyzer–detector respectively. The sample was mounted in a furnace consisting of split Nichrome heaters surrounded by a cylindrical aluminum shell. Temperatures were controlled to a relative precision of ±1 K with a Chromel-Alumel thermocouple mounted close to the sample; however, the absolute accuracy was probably no better than ±5 K. Scans were performed at 0·05° intervals over each of the peak positions previously observed within an angular range 2θ of 25–127° at 295, 364, 419 and 723 K. In addition, scans of the 400 and 440 reflections (pseudocubic indices) were made at a number of intermediate temperatures. Except for the 295 K scan, longer counting rates were used for the weaker peaks to improve statistics. A feature of the data was the very low background counting rate, about 10 counts min^{-1}, or about 0·5% of the strongest peak intensity.

3. Results

3.1. *Electrical, magnetic, and thermal behavior*

The results of electrical-resistivity measurements on a $BaBiO_3$ crystal are shown in Fig. 1. Several other crystals were studied, and the electrical behavior was found to be very similar. Over the range 100 to 473 K semiconducting behavior was observed with an activation energy of about 0·2 eV. There is some indication of a discontinuity at around 400 K. Between 4·2 and 100 K the resistivity was greater than 10^6 Ω m and too high to be determined with our technique. The

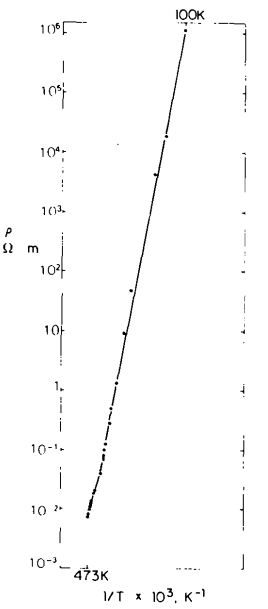

Fig. 1. Electrical resistivity of $BaBiO_3$ as a function of temperature.

resistivity of a sintered pellet was found to be about 10^4 times higher than that of the crystals, which was attributed to high-resistivity grain boundaries. This pellet remained semiconducting to at least 973 K.

The room-temperature magnetic susceptibility was found to be 17×10^{-5} mol^{-1}, in good agreement with the result of Nakamura *et al.* (1971). This susceptibility is well within the range anticipated for diamagnetism. There is a gradual increase in the susceptibility with decreasing temperature which is probably due to a very small amount of paramagnetic impurity.

Transitions were sought over the range 150 to 770 K by DSC. Only one transition, at about 405 K, was found. The sharpness and hysteresis associated with this transition indicates that it is first order. An accurate determination of the transition temperature was not achieved due to the hysteresis. High-temperature TGA experiments in air showed a reversible weight loss beginning at about 925 K.

3.2. *X-ray data*

High-temperature Guinier X-ray photographs showed that $BaBiO_3$ transforms from monoclinic to rhombohedral at about 405 K. Furthermore, the compound appears to become cubic at about 750 K. However, this transition is rather gradual and probably second order, and an accurate transition temperature was not obtained here either. This transition was not revealed by either DTA or DSC experiments.

In view of the conflicting X-ray results recently reported by Khan *et al.* (1977) and Arpe & Müller-Buschbaum (1977), detailed attention was given to the characterization of the room-temperature phase. The former authors studied the $BaBiO_3$–$BaPbO_3$ system, and concluded that the correct unit cell was orthorhombic, with parameters $a \simeq b \simeq a_0\sqrt{2}$, $c \simeq a_0$, where a_0 is the lattice parameter of the simple pseudocubic perovskite cell. They were unable to detect any superstructure peaks resulting from doubling of the unit cell, and attributed the same negative observation to Shannon & Bierstedt (1970) and Cox & Sleight (1976*a*,*b*). This is incorrect; both sets of authors reported clear evidence of the doubling of the *c* axis, as did Thornton & Jacobson (1976, 1978).

The mistake made by Khan *et al.* (1977) is due to the X-ray peaks with *l* odd which reveal the doubling of the *c* axis being extremely weak. This is illustrated by the room-temperature data for $BaBiO_3$ given in Table 1, which lists observed *d* spacings and intensities together with those calculated for a body-centered monoclinic cell with $a = 6{\cdot}1814$, $b = 6{\cdot}1360$, $c = 8{\cdot}6697$ Å, $\beta = 90{\cdot}173°$, and the atomic positional parameters determined by Cox & Sleight (1976*a*). It can be seen that only three peaks with *l* odd are observed, and these are calculated to have no more than 0·3% the intensity of the strongest peak. This is because the atomic movements responsible for the doubling are essentially all oxygen shifts, but the X-ray scattering is dominated by Ba and Bi, of course. This is not the case for neutron

Table 1. *Observed and calculated X-ray d spacings and intensities for* $BaBiO_3$

hkl are indices based upon a body-centered monoclinic cell with $a = 6{\cdot}1814$, $b = 6{\cdot}1360$, $c = 8{\cdot}6697$ Å, and $\beta = 90{\cdot}173°$. *h'k'l'* refer to the equivalent face-centered cell described in § 3. Only those peaks with calculated intensities of 1 or greater are listed. N.O. denotes 'not observed'.

h k l	d_{obs}	d_{calc}	I_{calc}	I_{obs}	*h' k' l'*
1 0 $\bar{1}$	N.O.	5.0403	2	N.O.	1 $\bar{1}$ $\bar{1}$
1 1 0	4.1570	4.1568	169	m$^-$	2 0 0
0 0 2	4.3389	4.3349	80	m$^-$	0 0 2
2 0 0	3.0895	3.0907	489	s$_+$	2 $\bar{2}$ 0
1 1 $\bar{2}$	3.0752	3.0755	999	s$^+$	2 0 $\bar{2}$
1 1 2	3.0682	3.0690	1000	s^{++}	2 0 2
0 2 0		3.0680	494		2 2 0
2 1 $\bar{1}$	2.6318	2.6323	3	w^{--}	3 $\bar{1}$ $\bar{1}$
2 1 1	2.6276	2.6282	2	w^{--}	3 $\bar{1}$ 1
1 0 $\bar{3}$	2.6218	2.6210	3	w^{--}	1 $\bar{1}$ $\bar{3}$
2 0 $\bar{2}$	2.5199	2.5201	3	w^{--}	2 $\bar{2}$ $\bar{2}$
2 0 2	2.5132	2.5130	3	w^{--}	2 $\bar{2}$ 2
0 2 2	2.5045	2.5042	4	w^{--}	2 2 2
2 2 0	2.1773	2.1774	515	s$_+$	4 0 0
0 0 4	2.1664	2.1674	246	m$^+$	0 0 4
2 1 $\bar{3}$	N.O.	1.9988	1	N.O.	3 $\bar{1}$ $\bar{3}$
1 2 $\bar{3}$	N.O.	1.9928	2	N.O.	3 1 $\bar{3}$
3 1 0	1.9532	1.9533	17	w	4 $\bar{2}$ 0
2 2 $\bar{2}$		1.9474	20		4 0 $\bar{2}$
2 2 2		1.9441	22		4 0 2
1 1 4	1.9425	1.9420	21	w$^+$	2 0 4
1 3 0		1.9418	20		4 2 0
1 1 $\bar{4}$		1.9387	19		2 0 4
3 1 $\bar{2}$	1.7815	1.7827	209	m	4 $\bar{2}$ $\bar{2}$
3 1 2	1.7789	1.7789	213	m$^+$	4 $\bar{2}$ 2
2 0 4		1.7771	106		2 $\bar{2}$ 4
1 3 $\bar{2}$		1.7727	198		4 2 $\bar{2}$
2 0 4	1.7719	1.7721	99	s	2 $\bar{2}$ 4
1 3 2		1.7715	202		4 2 2
0 2 4		1.7702	208		2 2 4
1 0 $\bar{5}$	N.O.	1.6708	1	N.O.	1 $\bar{1}$ $\bar{5}$
4 0 0	1.5452	1.5454	77	m$^-$	4 $\bar{4}$ 0
2 2 4	1.5374	1.5377	151	m	4 0 4
2 2 4	1.5346	1.5345	151	m$^+$	4 0 4
0 4 0		1.5340	80		4 4 0
1 2 $\bar{5}$	N.O.	1.4656	1	N.O.	3 1 $\bar{5}$
4 0 $\bar{2}$	1.4534	1.4570	4	w$^-$	4 $\bar{4}$ $\bar{2}$
4 0 2		1.4542	5		4 $\bar{4}$ 2
3 1 4		1.4531	7		4 $\bar{2}$ 4
3 3 0		1.4516	7		6 0 0
3 1 4		1.4489	6		4 $\bar{2}$ 4
1 3 4		1.4469	8		4 2 4
0 4 2	1.4461	1.4461	7	w	4 4 2
1 3 4		1.4456	8		4 2 4
0 0 6		1.4450	3		0 0 6
4 2 0	1.3802	1.3802	81	m$^-$	6 $\bar{2}$ 0
3 3 $\bar{2}$		1.3773	88		6 0 $\bar{2}$
3 3 2	1.3754	1.3756	89	m$^+$	6 0 2
2 4 0		1.3741	84		6 2 0
1 1 $\bar{6}$	1.3712	1.3723	84	m	2 0 6
1 1 6		1.3706	85		2 0 6
4 2 $\bar{2}$	1.3150	1.3161	3	w^{--}	6 $\bar{2}$ 2
4 2 2		1.3141	3		6 2 2
2 0 $\bar{6}$		1.3105	2		2 $\bar{2}$ 6
2 4 $\bar{2}$	1.3095	1.3103	2	w$^-$	6 $\bar{2}$ 2
2 4 2		1.3093	2		6 2 2
2 0 6		1.3075	2		2 2 6
0 2 6		1.3072	3		2 2 6
4 0 $\bar{4}$	1.2600	1.2601	35	w	4 $\bar{4}$ 4
4 0 4	1.2566	1.2565	36	w	4 4 4
0 4 4	1.2523	1.2521	74	w$_+$	4 4 4
5 1 0		1.2119	4		6 $\bar{4}$ 0
3 3 $\bar{4}$		1.2073	4		6 0 4
2 2 $\bar{6}$	1.2048	1.2051	3	w,b	4 0 6
3 3 4		1.2049	4		6 0 4
1 5 0		1.2037	4		6 4 0
2 2 6		1.2028	4		4 0 6
5 1 $\bar{2}$	1.1684	1.1681	53	w$^+$	6 $\bar{4}$ 2
5 1 2	1.1662	1.1663	54	m$^-$	6 $\bar{4}$ 2
4 2 $\bar{4}$		1.1656	50		6 $\bar{2}$ $\bar{4}$
3 1 6	1.1628	1.1632	49	m	4 $\bar{2}$ 6
4 2 4		1.1628	47		6 $\bar{2}$ 4
2 4 4		1.1612	51		6 2 4
3 1 $\bar{6}$		1.1601	52		4 $\bar{2}$ 6
1 5 $\bar{2}$		1.1600	50		6 4 $\bar{2}$
2 4 4	1.1599	1.1598	49	m$^+$	6 2 4
1 3 6		1.1597	48		4 2 6
1 5 2		1.1596	49		6 4 2
1 3 6		1.1587	50		4 2 6
4 4 0	1.0892	1.0887	47	w$_+$	8 0 0
0 0 8	1.0837	1.0837	22	w	0 0 8

scattering, and relatively strong peaks with l odd are observed, as previously reported.

Furthermore, the X-ray pattern shows a strong resemblance to the orthorhombic pattern of $BaPbO_3$. The underlying monoclinic symmetry is most clearly revealed by the presence of the three weak peaks $20\bar{2}$, 202 and 022, which correspond to splitting of the pseudocubic 111 reflection. In an orthorhombic cell, of the type described by Khan *et al.* (1977), this would split into only two such peaks.

The structure reported by Arpe & Müller-Buschbaum (1977) involves a statistical distribution of Ba and O atoms and bears little resemblance to the monoclinic structure, or as far as is known, to any other perovskite-type structure. The tetragonal c dimension, 4·518 Å, is substantially greater than any of the appropriately normalized monoclinic dimensions $a_m/\sqrt{2}$, $b_m/\sqrt{2}$ or $c_m/2$, or for that matter any of the normalized dimensions reported in the numerous studies already referenced. It is, however, close to that reported by Aurivillius (1943) for rapidly cooled oxygen-deficient material with the approximate composition $Ba_{0.8}Bi_{1.2}O_{2.6}$ ($a = 4{\cdot}36$, $c = 4{\cdot}49$ Å). It therefore appears likely that the crystals prepared by Arpe & Müller-Buschbaum were similarly oxygen-deficient.

3.3. *Neutron data*

The neutron patterns showed peaks characteristic of a face-centered cell with an edge of about 8·7 Å over the whole temperature range studied. As noted in our previous room-temperature study, this corresponds to a doubling of the cell edge a_0 of the simple perovskite structure, and is typical of many ordered perovskites of the type $A_2BB'O_6$. The symmetry change noted on the X-ray photographs at about 405 K was clearly revealed by substantial changes in intensity of some of the neutron peaks. The most striking example of this is the pseudocubic 440 reflection, as illustrated in Fig. 2. Furthermore, the data show hysteresis effects in the temperature range 375–415 K, as exemplified by significant intensity differences in the scans performed at 402 K during heating and cooling cycles.

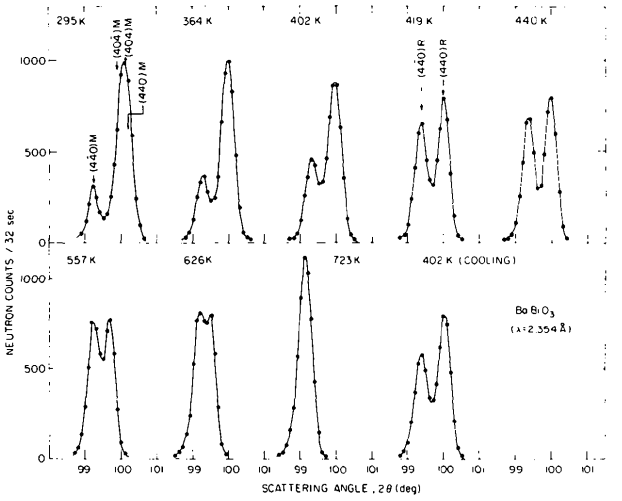

Fig. 2. Temperature dependence of the pseudocubic 440 reflection ($2a_0$ cell) of $BaBiO_3$.

The neutron diffraction patterns above and below the 405 K transition can be indexed in terms of conventional primitive rhombohedral ($a_r \simeq a_0\sqrt{2}$, $\alpha_r \simeq 60°$) and body-centered monoclinic ($a_m \simeq b_m \simeq a_0\sqrt{2}$, $c_m \simeq 2a_0$, $\beta \simeq 90°$) cells respectively. Application of Glazer's (1972, 1975) method for classifying octahedral tilts in ABO_3 perovskites to the $A_2BB'O_6$ structure with space group $Fm3m$ suggests the tilt systems $a^-a^-a^-$ (space group $R\bar{3}$) and $a^-a^-c^0$ (space group $I2/m$) respectively. It should be noted that the rhombohedral space group derived for the ABO_3 case has $R\bar{3}c$ symmetry, with only a single set of sites for the B atoms.

The conventional cells described above have different volumes and their relationship with the pseudocubic cell

Table 2. *Atomic positions and symmetry constraints on anisotropic temperature factors β_{ij} for* $BaBiO_3$ *with space group* R_F3

The β_{ij}'s are expressed in the temperature factor as $\exp[-(h^2\beta_{11} + k^2\beta_{22} + l^2\beta_{33} + 2hk\beta_{12} + 2hl\beta_{13} + 2kl\beta_{23})]$. ω is the octahedron tilt angle about the pseudocubic [111] axis ($\Delta \simeq -\Delta' \simeq \tan\omega/4\sqrt{3}$). Models and constraints are as described in the text. Scattering amplitudes for Ba, Bi and O are 0·512, 0·852, and $0{\cdot}580 \times 10^{-14}$ m respectively.

Ba	in 8(*c*)	x	x	x	$\beta_{11} = \beta_{22} = \beta_{33}$,
Bi(1)	in 4(*a*)	0	0	0	$\beta_{12} = \beta_{13} = \beta_{23}$
Bi(2)	in 4(*b*)	0·5	0·5	0·5	
O	in 24(*f*)	u	Δ	Δ'	$\beta_{11}, \beta_{22}, \beta_{33}$, $\beta_{12}, \beta_{13}, \beta_{23}$

	A (419 K, constrained)	*B* (419 K, unconstrained)	*C* (723 K, constrained)
Ba: x	0·25	0·2513 (9)	0·25
O: u	0·2610 (3)	0·2609 (4)	0·2604 (3)
O: Δ	0·0232 (2)	0·0239 (8)	0·0151 (2)
O: Δ'	−0·0232	−0·0223 (9)	−0·0151
Ba: β_{11}	0·0031 (4)	0·0032 (4)	0·0063 (5)
Ba: β_{12}	0·0	0·0001 (4)	0·0
Bi(1): β_{11}	0·0027 (6)	0·0033 (6)	0·0046 (6)
Bi(1): β_{12}	0·0	0·0004 (8)	0·0
Bi(2): β_{11}	0·0016 (6)	0·0016 (6)	0·0031 (5)
Bi(2): β_{12}	0·0	0·0008 (8)	0·0
O: β_{11}	0·0014 (5)	0·0020 (5)	0·0029 (6)
O: β_{22}	0·0104 (4)	0·0096 (24)	0·0187 (6)
O: β_{33}	0·0104	0·0121 (24)	0·0187
O: β_{12}	0·0	0·0000 (12)	0·0
O: β_{13}	0·0	−0·0011 (3)	0·0
O: β_{23}	0·0	0·0022 (5)	0·0
a (Å)	8·7094 (2)	8·7092 (2)	8·7449 (3)
α (°)	90·265 (1)	90·267 (1)	90·072 (5)
R_I (%)	3·0	1·9	2·2
R_P (%)	8·9	8·7	8·8
R_{wP} (%)	12·5	12·2	14·0
R_E (%)	9·4	9·3	9·5

is difficult to visualize. We have accordingly used non-conventional cells $R_F\bar{3}$ (the subscript denoting face-centering) and $F2/m$ based upon the doubled perovskite cell ($a \simeq 2a_0$). The relationship between the cells is shown in Fig. 3. The corresponding atomic positions are listed in the top parts of Tables 2 and 3, respectively, together with the symmetry constraints on the anisotropic thermal parameters β_{ij}. A more detailed discussion of the geometrical features of rhombohedral perovskites including the transformation matrices can be found in Megaw & Darlington (1975).

Structural analysis was carried out by means of the profile-refinement technique (Rietveld, 1969*a*,*b*; Hewat, 1973*a*).

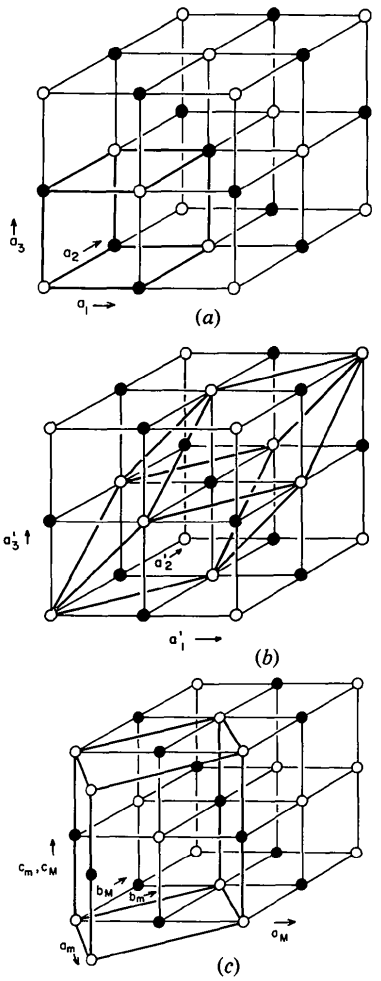

Fig. 3. Relationship between the doubled ($2a_0$) face-centered cells and the simpler cells described in the text. Open and closed circles depict B and B' atoms, respectively, in the ordered perovskite $A_2BB'O_6$. (*a*) $Fm3m$ cell. Simple perovskite cell with edge a_0 is shown in heavy outline. (*b*) $R_F\bar{3}$ cell. Primitive $R\bar{3}$ cell ($a_r \simeq a_0\sqrt{2}$, $\alpha_2 \simeq 60°$) is shown in heavy outline. (*c*) $F2/m$ cell. Body-centered $I2/m$ cell ($a_m \simeq b_m \simeq a_0\sqrt{2}$, $c_m = 2a_0$, $\beta \simeq 90°$) is shown in heavy outline.

4. Structures

419 K

The best results were obtained in the refinement of the 419 K data. An important feature of these data was the presence of a small but significant peak at the pseudocubic 111 position (Fig. 4, top). This is not permitted in the space group $R\bar{3}c$ due to the c glide plane and refinement was therefore based upon the space group $R\bar{3}$, which is the only centrosymmetric rhombohedral subgroup of $R\bar{3}c$.

Table 3. *Atomic positions and symmetry constraints on anisotropic temperature factors β_{ij} for* $BaBiO_3$ *with space group F2/m.*

The matrix for transforming atomic coordinates from the $I2/m$ cell previously used has the elements ($\frac{1}{2}$, $\frac{1}{2}$, 0; $\frac{1}{2}$, $\frac{1}{2}$, 0; 0, 0, 1). ω is the octahedron tilt about the pseudocubic [110] axis ($\Delta_1 \simeq -\Delta_2' \simeq \tan \omega/4\sqrt{2}$). Models and constraints are as described in text. Scattering amplitudes are as in Table 2. The differences in a, b, and c for the two sets of 295 K data arise from small errors in the neutron wavelengths.

Ba	in 8(*i*)	x	$\bar{x}$	z	$\beta_{11} = \beta_{22}, \beta_{33}$, $\beta_{12}, \beta_{13} = -\beta_{23}$
Bi(1)	in 4(*a*)	0	0	0	
Bi(2)	in 4(*b*)	0·5	0·5	0·5	
O(1)	in 8(*i*)	Δ_1	$-\Delta_1$	u_1	
O(2)	in 16(*j*)	u_2	Δ_2	Δ_2'	$\beta_{11}, \beta_{22}, \beta_{33}$, $\beta_{12}, \beta_{13}, \beta_{23}$

	A 295 K (old)	*B* 295 K	*C* 364 K
Ba:x	0·2523 (6)	0·2520 (8)	0·2508 (9)
Ba:z	0·2470 (16)	0·2496 (21)	0·2547 (21)
O(1):Δ_1	0·0316 (2)	0·0312 (4)	0·0306 (4)
O(1):u_1	0·2604 (4)	0·2604 (6)	0·2616 (5)
O(2):u_2	0·2604	0·2604	0·2616
O(2):Δ_2	0·0	0·0	0·0
O(2):Δ_2'	−0·0316	−0·0312	−0·0306
Ba:β	0·0025 (3)	0·0019 (5)	0·0037 (6)
Bi(1):β	0·0040 (7)	0·0014 (8)	0·0032 (9)
Bi(2):β	−0·0005 (6)	0·0029 (8)	0·0024 (8)
O(1):β_{11}	0·0078 (4)	0·0081 (5)	0·0100 (6)
O(1):β_{22}	0·0078	0·0081	0·0100
O(1):β_{33}	0·0020 (7)	0·0006 (8)	0·0026 (9)
O(2):β_{11}	0·0020	0·0006	0·0026
O(2):β_{22}	0·0078	0·0081	0·0100
O(2):β_{33}	0·0078	0·0081	0·0100
a (Å)	8·7371 (3)	8·7071 (5)	8·7123 (5)
b (Å)	8·7371	8·7071	8·7123
c (Å)	8·6945 (4)	8·6641 (6)	8·6761 (7)
α (°)	89·893 (6)	89·899 (5)	89·906 (7)
β (°)	90·107	90·101	90·094
γ (°)	90·406 (3)	90·401 (5)	90·372 (6)
R_I (%)	2·6	3·9	7·9
R_P (%)	6·2	11·0	14·6
R_{wP} (%)	8·5	16·2	19·4
R_E (%)	4·0	13·4	9·1

Refinement was initially carried out under the constraints of the rigid-octahedron model with a [111] tilt axis, individual isotropic temperature factors and x(Ba) fixed at the ideal value of 0·25. This gave a quite satisfactory fit with R factors $R_I = 5{\cdot}5$, $R_P = 10{\cdot}8$, $R_{wP} = 14{\cdot}4$ and $R_E = 9{\cdot}4\%$. The first three are based upon integrated intensities, unweighted point-by-point intensities and weighted point-by-point intensities respectively, and R_E is the statistical or 'expected' value as defined by Rietveld (1969*a*,*b*) and Hewat (1973*a*). The actual profile fit, together with the difference plot, is shown in Fig. 4 (top). To show a reasonable amount of detail, several intermediate regions of the scan containing only background points have been omitted. Only the points actually used in the refinement have been plotted, and background has not been subtracted, as is frequently the case. Pseudocubic indices based upon the doubled ($2a_0$) cell are entered above the peaks, and those with odd indices which are mostly absent on X-ray patterns are clearly visible. The weak 111 reflection is also shown on an expanded (×10) intensity scale.

A marked improvement was obtained with an anisotropic O temperature factor subject to the constraints of $Fm3m$ symmetry as listed in Table 2, which introduces one extra parameter ($R_I = 3{\cdot}0$, $R_P = 8{\cdot}9$, $R_{wP} = 12{\cdot}5$, $R_E = 9{\cdot}4\%$). The results of this refinement are summarized in Table 2 (column *A*). Further refinements in which some or all of the rigid-octahedron β_{ij} and Ba:x constraints were lifted resulted in very little change as can be seen from the results obtained with no constraints at all other than those imposed by $R\bar{3}$ symmetry (Table 2, column *B*). The corresponding plot of the thermal ellipsoids is shown in Fig. 5. It is interesting to note that in this case, the shift of the Ba atom from its ideal position is hardly significant, and that with the exception of β_{23} for O, all the deviations from the constrained anisotropic model are within the estimated errors. It is therefore unlikely that the small decreases in R factors represent a significant improvement over the constrained model. The profile fit for the latter is shown in Fig. 4 (middle), and some of the discrepancies observed for the isotropic model are seen to be significantly reduced, in particular the 422 reflection.

Refinement was also carried out in the space groups $R\bar{3}c$ and $R\bar{3}m$. The former gave an appreciably worse set of R factors (6·1, 11·1 and 16·6%) with obvious discrepancies for reflections such as 111 which should be absent due to the glide plane, while $R\bar{3}m$ proved to be quite hopeless with R factors five times as high.

The structure of $BaBiO_3$ at 419 K can therefore be described very well in terms of the rigid-octahedron model with a [111] tilt axis, ordering of the Bi atoms, and relatively large amplitudes of vibration [$\langle u_{ii}^2\rangle^{1/2} = (\beta_{ii}/2\pi^2 a_i^{*2})^{1/2}$] for O atoms perpendicular to the Bi—O bonds (≃0·2 Å) compared to those along the bonds and also those of the metal atoms (≃ 0·1 Å).

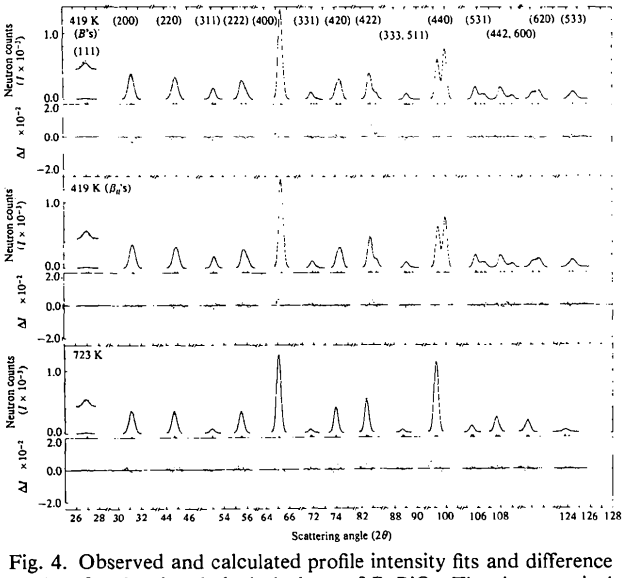

Fig. 4. Observed and calculated profile intensity fits and difference plots for the rhombohedral phase of $BaBiO_3$. The short vertical lines below the peaks indicate the calculated peak positions. The lowest-angle peak (111) is also shown plotted on an expanded intensity scale (×10). Top: 419 K, rigid-octahedron model, isotropic B's; pseudocubic ($2a_0$) indices are given above peaks. Middle: 419 K, rigid-octahedron model, anisotropic β_{ii}'s subject to $Fm3m$ symmetry constraints. Bottom: 723 K, rigid-octahedron model, anisotropic β_{ii}'s subject to $Fm3m$ symmetry constraints.

723 K

Inspection of the neutron diffraction pattern revealed that the symmetry was still lower than cubic and that most of the odd reflections were considerably diminished in intensity. The 111 reflection was still present, and refinement was accordingly carried out in space group $R\bar{3}$ once again. A reasonable fit was

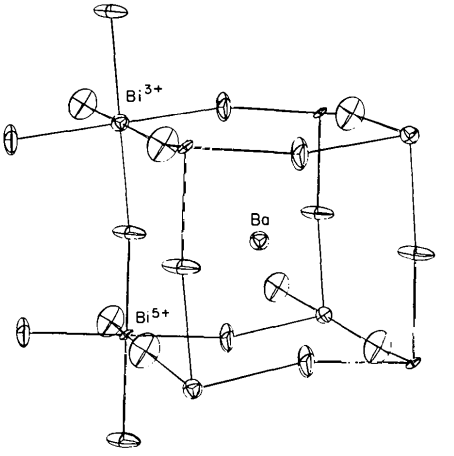

Fig. 5. *ORTEP* thermal-ellipsoid plot of $BaBiO_3$ at 419 K showing one octant of the face-centered cell. Parameters are as in Table 4, column *B*.

obtained with the rigid-octahedron model, isotropic temperature factors, and Ba in its ideal position (R's 7·0, 12·2, 17·9%; R_E 9·5%) but, just as at 419 K, a marked improvement was obtained with anisotropic O temperature factors subject to the constraints of $Fm3m$ symmetry (R's 2·2, 8·8, 14·0%; R_E 9·5%). The results of this refinement are summarized in Table 2 (column C) and the profile fit is shown in Fig. 4 (bottom). Further refinements without some or all of the above constraints did not improve matters much, and in many cases failed to converge because of large correlation effects.

The chief differences at this temperature compared to 419 K are a decrease in Δ, which reflects a decrease in the [111] tilt angle, and an increase in the r.m.s. amplitudes, by roughly the same factor (about $\sqrt{2}$). In addition, the rhombohedral angle α is much closer to 90°. All of these features may be taken as an indication of an impending transition to cubic symmetry.

295 K

The neutron data obtained at 295 K in the present study were refined in terms of the face-centered cell rather than the body-centered $I2/m$ cell used in the previous study (Cox & Sleight, 1976*a*). A rigid-octahedron model with a [110] tilt axis and isotropic temperature factors for each atom [the values for O(1) and O(2) were not constrained to be the same] gave R factors of 5·3, 11·9, and 17·0% (R_E 13·4%). For comparison, the old data were also refined in this way. The R factors of 2·9, 6·3, and 8·7% (R_E 4·0%) in this case reflect the much better counting statistics, but almost all the parameters agreed to within one standard deviation, the exceptions being the temperature factors of the two Bi atoms, where the differences were closer to 4σ. The results are also in good agreement with those of Thornton & Jacobson (1978).

Both sets of data were also refined with anisotropic O temperature factors constrained to $Fm3m$ symmetry, *i.e.* $O(1):\beta_{11} = O(1):\beta_{22} = O(2):\beta_{22} = O(2):\beta_{33}$; $O(1):\beta_{33} = O(2):\beta_{11}$. A small decrease in R factors was obtained even though the total number of parameters is the same as in the isotropic refinement. The results are given in Table 3 in columns A and B. The corresponding profile fits are illustrated in Fig. 6 (top and middle). Removal of some or all of the other constraints resulted in further slight improvements as the number of parameters grew, but the significance of these results was judged to be questionable. For example, refinement of the old data with only $F2/m$ symmetry constraints on the oxygen β_{ij}'s yielded R factors of 2·1, 5·4, and 7·6% with the following values: $O(1):\beta_{11} = \beta_{22} = 0{\cdot}0067\ (12)$, $\beta_{33} = 0{\cdot}0025\ (14)$; $\beta_{13} = -\beta_{23} = -0{\cdot}0006\ (13)$; $O(2):\beta_{11} = 0{\cdot}0015\ (9)$, $\beta_{22} = 0{\cdot}0105\ (14)$, $\beta_{33} = 0{\cdot}0080\ (9)$; $\beta_{12} = \beta_{11} = 0{\cdot}0047\ (8)$, $\beta_{13} = 0{\cdot}0015\ (15)$, $\beta_{23} = -0{\cdot}0037\ (17)$. These values indicate that the simple two-parameter approximation is quite reasonable.

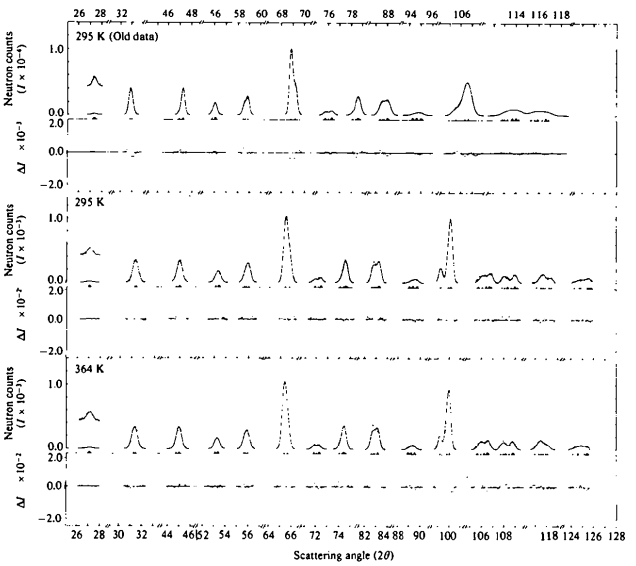

Fig. 6. Observed and calculated profile intensity fits and difference plots for the monoclinic phase of $BaBiO_3$; rigid-octahedron model, anisotropic β_{ij}'s subject to $Fm3m$ symmetry constraints. The lowest-angle peak (111) is also shown plotted on an expanded intensity scale (×10). Top: 295 K, previous data, spectrometer configuration as described in text, wavelength 2·47 Å; the 2θ scale for this plot is at the top. Middle: 295 K, present data. Bottom: 364 K.

364 K

Inspection of the X-ray and neutron diffraction patterns indicated that the space group and basic structure were the same as at 295 K. Refinement based upon the rigid-octahedron isotropic-temperature-factor model gave a fit distinctly poorer than in all the previous cases, with R factors of 8·7, 14·8, and 19·7% (R_E 9·1%). The constrained two-parameter anisotropic model gave only a marginal improvement (Table 3, column C), with substantial discrepancies, at some reflections, notably $4\bar{4}0$. This can be seen in Fig. 6 (bottom). Removal of the oxygen β_{ij} constraints gave better R factors (6·3, 12·3, 17·0%; R_E 8·9%), and in particular a much better fit for $4\bar{4}0$, with the following values: $O(1):\beta_{11} = \beta_{22} = 0{\cdot}0084\ (20)$, $\beta_{33} = 0{\cdot}0051\ (17)$; $\beta_{12} = 0{\cdot}0081\ (24)$, $\beta_{13} = -\beta_{23} = 0{\cdot}0008\ (15)$; $O(2):\beta_{11} = 0{\cdot}0019\ (12)$, $\beta_{22} = 0{\cdot}0090\ (17)$, $\beta_{33} = 0{\cdot}0147\ (16)$; $\beta_{12} = 0{\cdot}0100\ (4)$, $\beta_{13} = -0{\cdot}0104\ (22)$, $\beta_{23} = -0{\cdot}0126\ (26)$. The β_{ij} matrix is not positive-definite, but it is nevertheless interesting to note that the diagonal terms are comparable to both those at 295 K, and those in the rhombohedral phase at 419 K, whereas the off-diagonal terms are much larger. This is probably an indication that the simple harmonic model is not a good approximation in the vicinity of the transition.

5. Temperature dependence of lattice parameters

As pointed out by Hewat (1973*b*) and Young, Mackie & Von Dreele (1977), an additional benefit of profile refinement is that the lattice parameters are usually determined to a high degree of precision. The refined values at 295, 364, 419, and 723 K are plotted in Fig. 7, together with values determined from scans of the 440 and 440 reflections at a number of temperatures in the rhombohedral region. The data indicate a first-order transition with a volume discontinuity of about 0·2% occurring at about 400 K. By extrapolation of the curve for the rhombohedral angle, α_R, the rhombohedral–cubic phase transition is estimated to take place between 750 and 800 K.

The monoclinic–rhombohedral transition is also characterized by a decrease in the width of the pseudo-cubic 400 peak, which is plotted as a function of temperature in Fig. 8. In the monoclinic region, this is a composite of two reflections about 0·3–0·4° apart, which coalesce into a single peak in the rhombohedral region. There is also an indication of some hysteresis between 400 and 420 K.

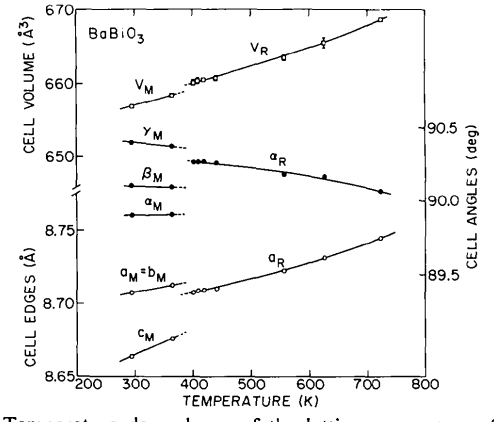

Fig. 7. Temperature dependence of the lattice parameters of the face-centered monoclinic and rhombohedral unit cells of $BaBiO_3$.

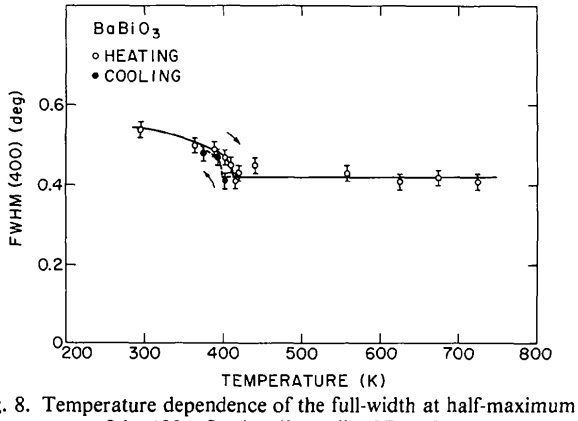

Fig. 8. Temperature dependence of the full-width at half-maximum of the 400 reflection ($2a_0$ cell) of $BaBiO_3$.

6. Profile resolution

In most of the versions of the profile-refinement program currently being used, the variation of peak widths (FWHM) as a function of Bragg angle is approximated by the expression $H^2(\theta) = U\tan^2\theta + V\tan\theta + W$, where U, V, and W are parameters of the refinement. The functions $H(\theta)$ obtained at each of the four temperatures are quite similar, the two extremes being shown by the solid lines in Fig. 9. In contrast, the curve obtained in the refinement of the old room-temperature data is markedly different (Fig. 9, broken line) because of differences in the geometrical configurations of the two experiments. The principal changes in the present experiment were the use of looser collimation in the monochromator-to-sample position (40′ instead of 20′), and the use of the pyrolytic-graphite analyzer in the 004 rather than the 002 setting. The former results in somewhat inferior resolution at low angles, while the latter gives clearly superior resolution at high angles. Based on the results of the refinements given in Table 3, it is difficult to make a direct comparison due to the different counting statistics and angular ranges of the two sets of data. However, in general, the 004 analyzer setting would certainly appear to be advantageous if some decrease in counting statistics can be tolerated, particularly when there are numerous overlapping peaks at high angles. The improved resolution should also enable a better estimate of the background to be made at high angles.

7. Discussion

The oxidation states in $BaBiO_3$ clearly remain Ba_2Bi^{3+}-$Bi^{5+}O_6$ from very low temperatures to at least 723 K. Although there is a first-order transition at about 405 K, there is no change in the valence situation at that transition, nor is there any change in the ordered

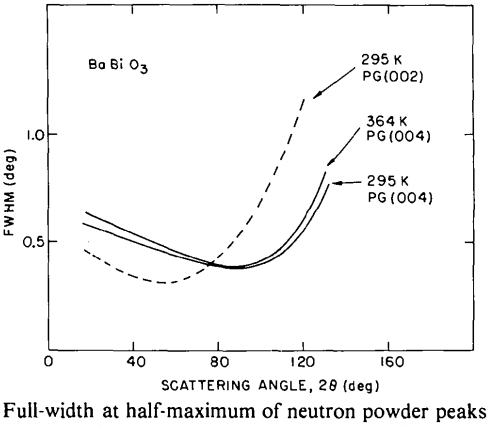

Fig. 9. Full-width at half-maximum of neutron powder peaks from $BaBiO_3$ as a function of scattering angle (2θ). Curves are calculated from the expression $H^2 = U\tan^2\theta + V\tan\theta + W$, where U, V and W are refined values. Solid and broken lines refer to the spectrometer configurations described in text.

arrangement of Bi^{3+} and Bi^{5+}. The Bi^{3+}—O and Bi^{5+}—O distances remain essentially unchanged (2·31 and 2·12 Å respectively) between 298 and 723 K, and these distances are easily rationalized on the basis of the assigned oxidation states (Cox & Sleight, 1976*a*).

The electrical and magnetic properties of $BaBiO_3$ are also consistent with the $Ba_2Bi^{3+}Bi^{5+}O_6$ valence situation. Although it has been suggested that $BaBiO_3$ is ferroelectric (Venevtsev, 1971; Fesenko *et al.*, 1972), we find no evidence to support ferroelectricity. The structural refinements are satisfactory in centrosymmetric space groups, and there is no significant drop in R values on going to noncentrosymmetric space groups. We failed to observe a piezoelectric effect on crystals, or a second-harmonic signal on powders. An attempt to decorate crystals also failed. Thus, it seems very unlikely that $BaBiO_3$ is ferroelectric at 298 K.

The crystallographic concepts of 'hard' and 'soft' structural features (Megaw, 1972, 1973) used to visualize the structures and phase transitions of perovskites and their lattice-dynamical counterparts (Cochran & Zia, 1968; Axe, 1971; Shirane, 1974) can readily be extended to the ordered perovskite $BaBiO_3$. The main distortion from the ideal ordered structure consists of tilting of the 'hard' structural units, the rigid BiO_6 octahedra. The directions and average angles of the tilts at the temperatures studied are summarized in Table 4. Although there is an abrupt change in direction at the 405 K transition, there is relatively little change in the tilt angle, which is regarded as a 'soft' parameter of the lattice. There is a substantial decrease in the tilt angle at 723 K which signals the approach of the high-temperature transition. The shift of the Ba atom from the ideal position is another 'soft' feature of the structure. There is a small but significant shift in the monoclinic phase at 295 K, but this becomes barely, if at all, detectable in the rhombohedral phase.

Also listed in Table 4 are the r.m.s. thermal amplitudes calculated from the data in Tables 2 and 3 with the constraints of *Fm3m* symmetry. Although one cannot attribute too much quantitative significance to these figures in view of the limited angular range of the data, the qualitative trends are nevertheless quite consistent with the above picture. The vibrational amplitudes of the cations and the oxygens along the Bi—O bond direction are comparable, but the perpendicular oxygen amplitude, which is another 'soft' parameter, is considerably larger. Similar effects have been noted in profile studies of some other perovskites (Hewat, 1973*b*, 1974; Ahtee & Hewat, 1975; Ahtee, Glazer & Hewat, 1978). According to the simple model proposed by Megaw (1972, 1973), the transformation from the rhombohedral to the cubic phase would occur when the perpendicular amplitudes of vibration of the O atoms are roughly equal to their static displacements. The latter are 0·29 and 0·20 Å at 419 and 723 K respectively. Although the thermal amplitudes in Table 4 are not reliable enough to allow a quantitative comparison to be made, the overall trend is qualitatively consistent with this model.

In lattice-dynamical language, the approach from the high-temperature side of this transition would correspond to the condensation of a soft R_{25} phonon in the cubic phase, as studied in detail in the perovskites $LaAlO_3$ (Axe, Shirane & Müller, 1969) and $PrAlO_3$ (Birgeneau, Kjems, Shirane & Van Uitert, 1974), for example. Both of these undergo a cubic–rhombohedral transition, but the rhombohedral phases have $R\bar{3}c$ symmetry since there is no ordering of the B cations. Indeed, the analogy between $PrAlO_3$ and $BaBiO_3$ extends even further, since at lower temperatures $PrAlO_3$ undergoes a first-order transition from rhombohedral to orthorhombic which involves exactly the same change in tilt axis from [111] to [110] with quite similar angles ($\omega = 8{\cdot}7$ and 9·4° respectively). Apart from the resulting symmetry of $BaBiO_3$ being monoclinic because of the ordering of Bi^{3+} and Bi^{5+}, there is a close resemblance between Fig. 7 of the present paper and Fig. 3 of Birgeneau *et al.* (1974) in the region of this transition. It is to be noted, however, that this first-order transition is not the same type as that found in a number of rare-earth perovskites such as $LaFeO_3$ (Geller & Raccah, 1970). In these cases, the low-temperature orthorhombic structure has the *Pbnm* symmetry of $GdFeO_3$ (Geller, 1956) which is characteristic of a great many distorted perovskites and involves an additional component to the tilt along the remaining axis, *i.e.* $a^-a^-c^+$ instead of $a^-a^-c^0$.

The origin of the first-order transition at 205 K in $PrAlO_3$ has been shown to lie in a delicate interplay between anharmonic lattice interactions, which slightly favor a rhombohedral structure, and the electron

Table 4. *Structural data for* $BaBiO_3$ *at various temperatures based on profile refinement of neutron powder data with the rigid-octahedron model and Fm3m symmetry constraints on the* β_{ij}*'s*

Temperature (K)	Pseudocubic tilt axis	Glazer notation	Tilt angle (°)	R.m.s. vibration amplitudes (Å) Ba	Bi(1)	Bi(2)	$O_{\parallel}$	$O_{\perp}$
295	[110]	$a^-a^-c^0$	10·1	0·09	0·07	0·11	0·05	0·18
364	[110]	$a^-a^-c^0$	9·8	0·12	0·11	0·10	0·10	0·20
419	[111]	$a^-a^-a^-$	9·1	0·11	0·10	0·09	0·07	0·20
723	[111]	$a^-a^-a^-$	6·0	0·16	0·13	0·11	0·11	0·27

phonon coupling between the Pr^{3+} $4f$ crystal-field levels and the R_{25} phonons, which prefers an orthorhombic structure (Harley, Hayes, Perry & Smith, 1973; Birgeneau *et al.*, 1974). A similar situation probably prevails in $BaBiO_3$ as far as the anharmonic interactions are concerned, but the competing interaction responsible for the first-order transition to lower symmetry has not yet been identified.

Helpful discussions with J. D. Axe and R. J. Birgeneau are gratefully acknowledged. The electrical data were obtained by J. L. Gillson.

References

AHTEE, M., GLAZER, A. M. & HEWAT, A. W. (1978). *Acta Cryst.* B**34**, 752–758.

AHTEE, M. & HEWAT, A. W. (1975). *Acta Cryst.* A**31**, 846–850.

ARPE, R. & MÜLLER-BUSCHBAUM, H. (1977). *Z. Anorg. Allg. Chem.* **434**, 73–77.

AURIVILLIUS, B. (1943). *Ark. Kemi Mineral. Geol.* **16A**, 1–13.

AXE, J. D. (1971). *Trans. Am. Cryst. Assoc.* **7**, 89–106.

AXE, J. D., SHIRANE, G. & MÜLLER, K. A. (1969). *Phys. Rev.* **183**, 820–823.

BIRGENEAU, R. J., KJEMS, J. K., SHIRANE, G. & VAN UITERT, L. G. (1974). *Phys. Rev. B*, **10**, 2512–2534.

COCHRAN, W. & ZIA, A. (1968). *Phys. Status Solidi*, **25**, 273–283.

COX, D. E. & SLEIGHT, A. W. (1976*a*). *Solid State Commun.* **19**, 969–973.

COX, D. E. & SLEIGHT, A. W. (1976*b*). *Proceedings of Conference on Neutron Scattering*, Gatlinburg, Tennessee, pp. 45–54, edited by R. M. MOON; available from the National Technical Information Service, Springfield, VA 22161.

FESENKO, E. G., SHUVAEVA, E. T. & GOL'TSOV, YU. I. (1972). *Kristallografiya*, **17**, 419–420; *Sov. Phys. Crystallogr.* **17**, 362–363.

GELLER, S. (1956). *J. Chem. Phys.* **24**, 1236–1239.

GELLER, S. & RACCAH, P. M. (1970). *Phys. Rev. B*, **2**, 1167–1172.

GLAZER, A. M. (1972). *Acta Cryst.* B**28**, 3384–3392.

GLAZER, A. M. (1975). *Acta Cryst.* A**31**, 756–762.

HAIR, J. TH. W. DE & BLASSE, G. (1973). *Solid State Commun.* **12**, 727–729.

HARLEY, R. T., HAYES, W., PERRY, A. M. & SMITH, S. R. P. (1973). *J. Phys. C*, **6**, 2382–2400.

HEWAT, A. W. (1973*a*). UK Atomic Energy Authority Research Group Report RRL 73/897 (unpublished).

HEWAT, A. W. (1973*b*). *J. Phys. C*, **6**, 2559–2572.

HEWAT, A. W. (1974). *Ferroelectrics*, **7**, 83–85.

KHAN, Y., NAHM, K., ROSENBERG, M. & WILLNER, H. (1977). *Phys. Status Solidi A*, **39**, 79–88.

LAWTON, S. L. & JACOBSON, R. A. (1966). *Inorg. Chem.* **5**, 743–749.

LONGWORTH, G. & DAY, P. (1976). *Inorg. Nucl. Chem. Lett.* **12**, 451–453.

MEGAW, H. D. (1972). *J. Phys.* (*Paris*), **33** (Suppl. *C*2), 2–5.

MEGAW, H. D. (1973). *Crystal Structures: A Working Approach.* Philadelphia: Saunders.

MEGAW, H. D. & DARLINGTON, C. N. W. (1975). *Acta Cryst.* A**31**, 161–173.

NAKAMURA, T. & CHOY, J.-H. (1977). *J. Solid State Chem.* **20**, 233–244.

NAKAMURA, T., KOSE, S. & SATA, T. (1971). *J. Phys. Soc. Jpn*, **31**, 1284.

ORCHARD, A. F. & THORNTON, G. (1977). *J. Chem. Soc. Dalton Trans.* pp. 1238–1240.

RIETVELD, H. M. (1969*a*). Reactor Centrum Nederland Research Report RCN 104 (unpublished).

RIETVELD, H. M. (1969*b*). *J. Appl. Cryst.* **2**, 65–71.

ROBIN, M. B. & DAY, P. (1967). *Adv. Inorg. Chem. Radiochem.* **10**, 247–422.

SCHOLDER, R., GANTER, K., GLASER, H. & MERZ, G. (1963). *Z. Anorg. Allg. Chem.* **319**, 375–386.

SHANNON, R. D. & BIERSTEDT, P. E. (1970). *J. Am. Ceram. Soc.* **53**, 635–636.

SHIRANE, G. (1974). *Rev. Mod. Phys.* **46**, 437–449.

SHUVAEVA, E. T. & FESENKO, E. G. (1969). *Kristallografiya*, **14**, 1066–1068; *Sov. Phys. Crystallogr.* **14**, 926–927.

SLEIGHT, A. W., GILLSON, J. L. & BIERSTEDT, P. E. (1975). *Solid State Commun.* **17**, 27–28.

THORNTON, G. & JACOBSON, A. J. (1976). *Mater. Res. Bull.* **11**, 837–841, 1054.

THORNTON, G. & JACOBSON, A. J. (1978). *Acta Cryst.* B**34**, 351–354.

VENEVTSEV, YU. N. (1971). *Mater. Res. Bull.* **6**, 1085–1096.

YOUNG, R. A., MACKIE, P. E. & VON DREELE, R. B. (1977). *J. Appl. Cryst.* **10**, 262–269.